

# Synthesis, Crystal Structure, and Physical Properties of the New Chain Alkalioxocuprate $K_3Cu_2O_4$

Katarina Đuriš,<sup>[a]</sup> Reinhard K. Kremer,<sup>[a]</sup> and Martin Jansen<sup>\*[a]</sup>

Dedicated to Professor Hanskarl Müller-Buschbaum on the Occasion of His 80th Birthday

**Keywords:** One-dimensional oxocuprates; Low-dimensional magnetism; Azide-nitrate route; Copper; Potassium

**Abstract.** Single crystals of  $K_3Cu_2O_4$  were prepared by the azide/nitrate route from respective stoichiometric mixtures of  $KN_3$ ,  $KNO_3$  and  $CuO$ , at 923 K, whereas powder samples were synthesised by solid state reaction of  $K_2O$ ,  $KCuO_2$  and  $CuO$ , sealed in gold ampoules and treated at 723 K. According to the single crystal structure analysis ( $Cmcm$ ,  $Z = 4$ ,  $a = 6.1234(1)$ ,  $b = 8.9826(2)$ ,  $c = 10.8620(2)$  Å,  $R_1 = 0.044$ ,  $R_2 = 0.107$ ), the main structural feature are undulating  $\overset{\circ}{\text{Cu}}\text{O}_2$  chains built up from planar, edge sharing  $\text{CuO}_4$  square units. From an

analysis of the Cu–O bond lengths, the valence state of either +2 or +3 can be unambiguously assigned to each copper atom. The magnetic susceptibilities show the dominance of antiferromagnetic (AFM) interactions. At high temperatures, the magnetic behaviour can be fitted with the Curie–Weiss law ( $\mu_{eff} = 1.84\mu_B$ ,  $\Theta = -105$  K). The experimental data can be very well described by a uniform Heisenberg chain with a nearest-neighbour spin intrachain interaction ( $J_{nn}$ ) of  $\sim 101$  K.

## Introduction

Low dimensional Mott insulating oxides show a wealth of unique physical properties that have attracted a lot of attention since their understanding is regarded the key for attaining insights in e.g. the mechanisms underlying the HTSC cuprates<sup>[1]</sup> or CMR manganates.<sup>[2]</sup> The corresponding families of compounds have a long history in solid state chemistry, and e.g. for the cuprates structural essentials and their relation to superconductivity were worked out by *Hk. Müller-Buschbaum*.<sup>[3,4]</sup> In particular, one-dimensional systems feature a number of special phenomena, as there are decoupling of spin and charge excitations,<sup>[5]</sup> spiral-magnetic order inducing ferroelectricity,<sup>[6]</sup> or spin-Peierls transitions.<sup>[7]</sup> Research in this field has suffered substantially from a lack of chemically well defined materials, exhibiting full translational symmetry. Especially the latter implication has impaired theoretical analyses, and has blurred experimental observations by inhomogeneities. In order to overcome such drawbacks, we have developed an efficient approach, the “azide/nitrate route”, for the solid state synthesis of intrinsically doped multinary transition metal oxides.<sup>[8]</sup> Most significantly, this method allows to precisely fix the oxygen content of the target compound, and the valence state of the transition metal, by the starting azide/nitrate ratio. At the

example of two new families of quasi one-dimensional intrinsically doped alkali metal manganates(II/III)<sup>[9–11]</sup> and cuprates(II/III)<sup>[12,13]</sup> we have proven this synthesis route to be quite versatile. The cuprate family has the general formula  $Na_{1+x}CuO_2$ . All members known so far,  $Na_3Cu_2O_4$ ,<sup>[12]</sup>  $Na_5Cu_3O_6$ <sup>[13]</sup> and  $Na_8Cu_5O_{10}$ ,<sup>[12]</sup> show complete charge order at room temperature within the one-dimensional cuprate anions, consisting of trans-edge sharing  $\text{CuO}_4$  squares.

Most interestingly, these compounds constitute the first unambiguous manifestations of Wigner crystals,<sup>[14]</sup> and they develop helical magnetic order at low temperatures.<sup>[15]</sup> The underlying frustration is on the one hand caused by the competition between antiferromagnetic (AFM) and ferromagnetic (FM) couplings within the chains and on the other hand by interchain exchange.

In order to modify the impact of the latter, we have started to synthesise analogous cuprate chain compounds containing potassium as a bigger alkali metal cation. Among the potassium cuprates known so far ( $KCuO$ ,  $K_3Cu_2O_2$ ,  $K_3Cu_5O_4$ ,  $KCuO_2$ <sup>[16–19]</sup>) only  $KCuO_2$  features chains of edge-sharing plaquettes. However, copper in the oxidation state +3 does not bear any unpaired spin. Here we present a new oxocuprate,  $K_3Cu_2O_4$ , which contains copper in the oxidation states +2 and +3. We describe the synthesis, crystal structure determination and magnetic characterisation. As a marked structural difference compared to  $Na_3Cu_2O_4$ , the  $\overset{\circ}{\text{Cu}}\text{O}_2$  ribbons are not planar but undulating with a repetition period of four  $\text{CuO}_4$  squares. Our magnetic data characterise  $K_3Cu_2O_4$  as a one-dimensional AFM Heisenberg chain with uniform nearest neighbour spin interaction between  $\text{Cu}^{2+}\cdots\text{Cu}^{2+}$  cations, viz. between next-nearest neighbour copper sites along the  $\overset{\circ}{\text{Cu}}\text{O}_2$  strand. Inter-

\* Prof. Dr. M. Jansen  
Fax: +49-711-689-1502

E-Mail: M.jansen@fkf.mpg.de

[a] Max-Planck Institut für Festkörperforschung  
Heisenbergstr. 1

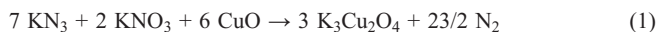
70569 Stuttgart, Germany

Supporting information for this article is available on the WWW under <http://dx.doi.org/10.1002/zaac.201100031> or from the author.

estingly, evidence for long-range AFM ordering has not been seen in heat capacity measurements.

## Experimental Section

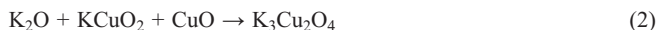
Starting materials for the preparation of the potassium cuprate were potassium azide, potassium nitrate (Riedel-De Haen AG Seelze, Hanover, 99.5 %) and CuO prepared by heating of  $\text{Cu}(\text{C}_2\text{O}_4)\cdot 0.5\text{H}_2\text{O}$  (Alfa Aesar, 98 %) in a flow of oxygen at 623 K for 20 h. The potassium azide was synthesised from aqueous  $\text{HN}_3$  and potassium carbonate (Sigma Aldrich, 99 %). The starting compounds were dried under vacuum ( $10^{-3}$  mbar) at 393 K overnight, mixed thoroughly in an agate mortar in a ratio according to Equation (1), and placed under argon in a closed steel container, provided with a silver inlay.



Black needle shaped single crystals of  $\text{K}_3\text{Cu}_2\text{O}_4$  were obtained applying the temperature schedule  $298 \rightarrow 533 \text{ K}$  ( $100 \text{ K}\cdot\text{h}^{-1}$ ),  $533 \rightarrow 673 \text{ K}$  ( $5 \text{ K}\cdot\text{h}^{-1}$ ),  $673 \rightarrow 923 \text{ K}$  ( $600 \text{ K}\cdot\text{h}^{-1}$ ), and subsequent annealing for 50 h at 923 K.

**Hazards:** The temperature control, as given above must be strictly followed. Rapid heating or running the reaction in a tightly closed container, could lead to dangerous explosion.

Using the azide/nitrate route,<sup>[8]</sup> the products always contained potassium cuprates(I) in addition to coarse crystalline  $\text{K}_3\text{Cu}_2\text{O}_4$ . To overcome this difficulty in the synthesis of single phase  $\text{K}_3\text{Cu}_2\text{O}_4$  powder, an alternative route according to Equation (2) was applied, by using  $\text{KCuO}_2$ , prepared according to<sup>[19]</sup> and  $\text{K}_2\text{O}$ , which was prepared from purified potassium by oxidation with molecular oxygen.<sup>[20]</sup>



Respective mixtures, including 2 mol-% excess of  $\text{K}_2\text{O}$ , were transferred to a gold ampoule, closed under argon atmosphere and treated at 723 K for 30 h. The obtained black powder, being very sensitive to air and moisture, was sealed and stored in glass ampoules under argon and all further handling was made in an inert atmosphere of purified argon.

X-ray powder studies were performed with a D8-Advance diffractometer (Bruker AXS, Karlsruhe, Germany) Cu- $K_{\alpha 1}$  radiation, provided from a Ge(111)-monochromated primary beam (Johannson monochromator). For refinement of the powder pattern, the program TOPAS<sup>[21]</sup> was used.

The single crystal diffraction data were collected with a smart APEX I three circle single crystal diffractometer (Bruker AXS, Karlsruhe, Germany) equipped with a CCD detector. Data collection and reduction were carried out with the Smart software package.<sup>[22]</sup> Intensities were corrected for absorption effects applying a semi-empirical method.<sup>[23]</sup> The structure was solved by direct methods and refined by full-matrix least-squares fitting with SHELXTL.<sup>[24]</sup>

Thermal analyses were carried out using a TG-DTA device (STA 409, Netzsch, Selb, Germany) coupled with a quadrupole mass spectrometer (QMG 421, Balzers). The samples were heated with a rate of  $10 \text{ K}\cdot\text{min}^{-1}$  in a corundum crucible, under dry argon.

Electron paramagnetic Resonance (EPR) was measured with a Bruker ER400XK microwave X-band spectrometer and a Bruker BE25 magnet equipped with a BH15 field controller, which was calibrated against Diphenylpicrylhydrazyl.

The magnetic susceptibilities were determined in the temperature range from 2 to 400 K, in discrete magnetic fields up to 7 T using a SQUID-Magnetometer (MPMS-XL, Quantum Design). The diamagnetic susceptibilities were determined using tabulated values.<sup>[25]</sup> The heat capacity of a pressed and sintered pellet sample (~ 20 mg) was measured with the relaxation method (PPMS, Quantum Design) between 2 and 250 K.

**Supporting Information** (see footnote on the first page of this article): X-ray powder data.

## Results and Discussion

### Synthesis, Crystal Structure

Single crystals of  $\text{K}_3\text{Cu}_2\text{O}_4$  were prepared via the azide/nitrate route, whereas the phase pure powders were obtained by classical solid state reaction. The TG-DTA measurements did not show any chemical reaction or phase transition during heating up to 923 K, where decomposition occurs. The crystal structure of the title compound was determined from single crystal data collected at 298 K, where it was found that  $\text{K}_3\text{Cu}_2\text{O}_4$  crystallises orthorhombic with the space group  $Cmcm$  (No.63).

Details and results of the structure refinement are given in Table 1, Table 2, and Table 3, interatomic distances, coordination numbers (CN), effective coordination numbers (ECOn) and mean fictive ionic radii (MEFIR) for  $\text{K}_3\text{Cu}_2\text{O}_4$  in Table 4. The collected powder diffraction pattern for  $\text{K}_3\text{Cu}_2\text{O}_4$  is shown in Figure 1, and the results obtained from the Rietveld refinement are given in Table 5. For the Rietveld refinement atomic coordinates obtained from the single crystal analysis were used.

According to the single-crystal structure analysis,  $\text{K}_3\text{Cu}_2\text{O}_4$  is isostructural to the Ni- and Pt-analogues,<sup>[26]</sup> and shows a fully charge-ordered copper partial structure. The most prominent structural feature are buckled one-dimensional  $_{\infty}\text{CuO}_2$  ribbon chains, which are build up from planar, edge-sharing  $\text{CuO}_4$  plaquettes (Figure 2a). From the analysis of the Cu–O bond lengths, valence states of either +2 or +3 can be unambiguously assigned to each copper atom ( $d(\text{Cu}^{2+}\text{–O}) = 1.939(3) \text{ \AA}$ ,  $d(\text{Cu}^{3+}\text{–O}) = 1.851(3) \text{ \AA}$ ).

In  $\text{K}_3\text{Cu}_2\text{O}_4$  the O–Cu–O angles in the  $\text{CuO}_4$  square units deviate from the ideal 90° due to variation of oxidation states of  $\text{Cu}^{\text{II}}$  and  $\text{Cu}^{\text{III}}$ , as well as due to the way, how these units are connected. The chains extend along the  $c$ -axis. The dihedral angle between two  $\text{CuO}_4$  square units is 155.7° (Figure 2a). This is in contrast to the sodium cuprates ( $\text{Na}_{1+x}\text{CuO}_2$ ), where the  $_{\infty}\text{CuO}_2$  chains are nearly flat with dihedral angles between two  $\text{CuO}_4$  square units approaching 180°. Different views of the crystal structure are given in Figure 2b.

The potassium ions occupy two crystallographically independent sites with four- and sixfold coordination (Figure 2c). K1 connects three  $_{\infty}\text{CuO}_2$  ribbons, with bonds to two oxygen atoms from each ribbon forming distorted prism (Figure 2c). K2 is equidistant with four oxygen atoms of two neighbouring  $_{\infty}\text{CuO}_2$  ribbons, forming a pyramid where K2 is situated on the top of the pyramid.

**Table 1.** Crystal data and structure refinement for  $K_3Cu_2O_4$ .

Space group (no.); $Z$	$Cmcm$ (63), 4
Cell parameters / $\text{\AA}$ (single crystal data)	$a = 6.1275(4)$ $b = 8.9908(7)$ $c = 10.8708(8)$
Volume / $\text{\AA}^3$	598.88(8)
$M_r$ /g·mol $^{-1}$	308.38
Calculated density /g·cm $^{-3}$	3.42
Temperature	298 K
Crystal form, colour	Needle shape, black
Crystal size /mm	0.25 × 0.10 × 0.08
Diffractometer	Bruker AXS, APEX SMART CCD
Monochromator	Graphite
X-ray radiation/ $\lambda$ / $\text{\AA}$	Mo- $K_{\alpha}$ , 0.71073
$\theta$ range /°	3.42 to 36.85
Index range	$-9 \leq h \leq 9$ $-14 \leq k \leq 14$ $-17 \leq l \leq 17$
Absorption correction	Multi-scan, SADABS <sup>[23]</sup>
Total no. reflections $N_{\text{all}}$	4609
Independent reflections $N$	725
Reflections $N'$ with $I > 2\sigma(I)N'$	704
Absorption coefficient/ $\mu$ / $\text{mm}^{-1}$	9.110
$F(000)$	588
Refinement method	Full-matrix least-squares on $F^2$
Weighting scheme	$w = 1 / [\sigma^2(F_o^2) + (0.0190P)^2 + 8.8769P]$ where $P = (F_o^2 + 2F_c^2)/3$
Goodness-on-fit on $F^2$	1.376
$R_1$ ( $N'$ ; N)	0.0429; 0.0439
$wR_2$ ( $N'$ ; N)	0.1066; 0.1070
Deposition no. <sup>[27]</sup>	CSD-380487

**Table 2.** Atomic coordinates and isotropic displacement parameters / $\text{\AA}^2$  for  $K_3Cu_2O_4$ .

Atom	Site	$x$	$y$	$z$	$U_{\text{eq}}$
Cu1	4a	0	0	0	0.0165(2)
Cu2	4c	0	0.0607(1)	1/4	0.0148(2)
K1	8f	0	0.3476(2)	0.0676(1)	0.0236(3)
K2	4c	0	0.6943(2)	1/4	0.0226(3)
O	16h	0.2952(5)	0.4377(4)	0.8859(3)	0.0234(6)

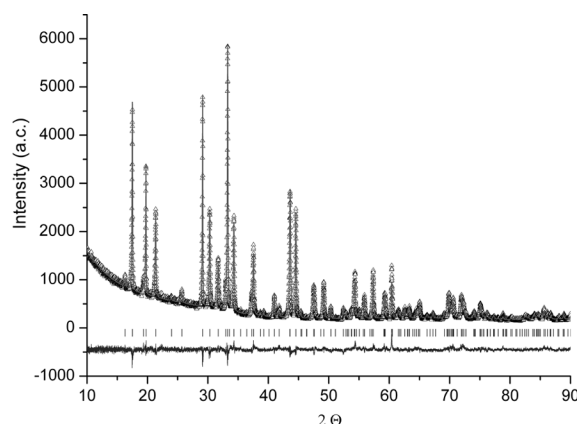
**Table 3.** Anisotropic displacement parameters ( $\times 10^{-2}$ ) / $\text{\AA}^2$  for  $K_3Cu_2O_4$ .

Atom	$U_{11}$	$U_{22}$	$U_{33}$	$U_{12}$	$U_{13}$	$U_{23}$
Cu1	1.15(4)	2.41(4)	1.39(4)	0	0	-0.37(3)
Cu2	1.27(4)	1.69(4)	1.49(4)	0	0	0
K1	1.98(5)	2.38(5)	2.74(6)	0	0	0.55(5)
K2	1.69(7)	2.59(8)	2.49(8)	0	0	0
O	1.2(1)	4.2(2)	1.7(1)	-0.2(1)	-0.1(1)	-0.7(1)

The new oxocuprate(II,III)  $K_3Cu_2O_4$  can be understood as a member of the compositional series  $K_{1+x}CuO_2$  with  $x = 0.5$  and with the end member  $KCuO_2$  ( $x = 0$ ).<sup>[19]</sup> Both compounds have a similar arrangement of the oxygen atoms, but different

**Table 4.** Interatomic distances (in pm), naive coordination numbers (CN), effective coordination numbers (ECoN) and mean fictive ionic radii (MEFIR)<sup>[28]</sup> for  $K_3Cu_2O_4$ .

Atom	O	CN	ECoN	MEFIR
Cu1	185.1	4	4	45.1
Cu2	193.8	4	4	53.8
K1	269.3	6	5.8	138.0
	279.8			
	290.1			
K2	261.9	4	4	121.9
CN	6			
ECoN	5.9			
MEFIR	140			

**Figure 1.** Powder X-ray diffraction data of  $K_3Cu_2O_4$ , observed (triangles), theoretical pattern (grey solid line) and difference between experimental and calculated patterns (underneath line). Bragg positions used to calculate the theoretical pattern of  $K_3Cu_2O_4$  are marked by ticks.**Table 5.** Crystallographic data for  $K_3Cu_2O_4$  (obtained by Rietveld refinement).

Space group, $Z$	$Cmcm$ (No.63), 4
Lattice constants / $\text{\AA}$	$a = 6.1234(1)$ $b = 8.9826(2)$ $c = 10.8620(2)$
Cell volume / $\text{\AA}^3$	597.46
Crystal density /g·cm $^{-3}$	3.42
Wavelength / $\text{\AA}$	1.540598 (Germanium monochromator)
Range data collection ( $2\theta$ ) /°	10–90
Colour of powder	Black
$R_{\text{Bragg}}$	3.27 %
$R_p$	4.86 %
$R_{\text{wp}}$	6.56 %

distribution of the cations (Cu, K) upon the trigonal prismatic (K) and square planar voids (Cu) as can be seen in Figure 3.

### Physical Properties

The heat capacity of  $K_3Cu_2O_4$  in log-log plot is presented in Figure 4, where it was shown that there is no indication of

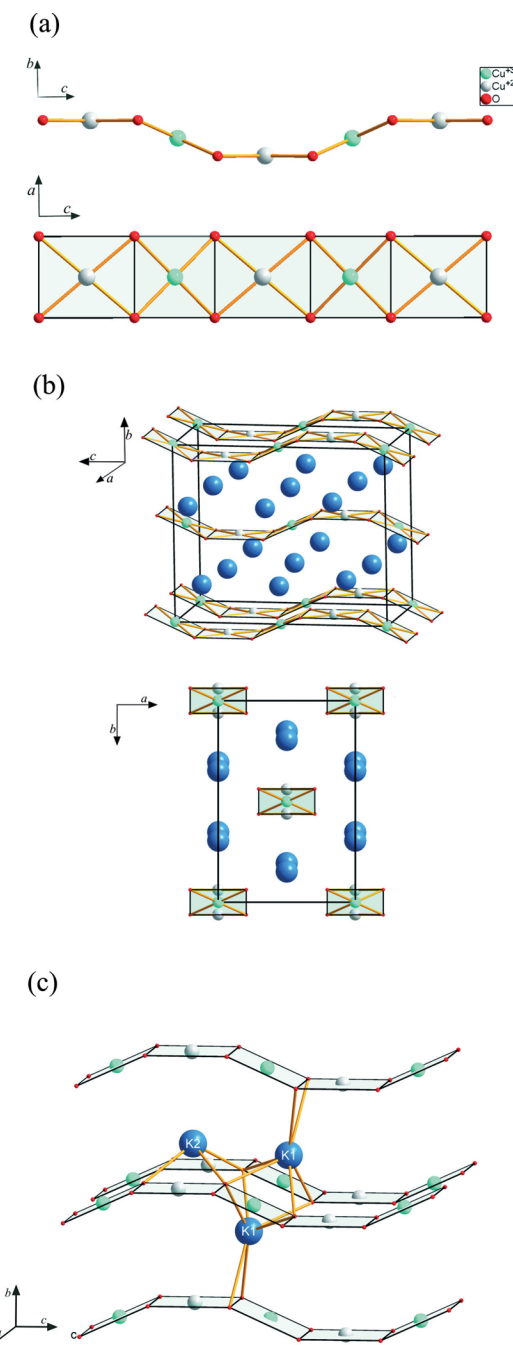


**Figure 2.** (a) Projections of a CuO<sub>2</sub> chain in K<sub>3</sub>Cu<sub>2</sub>O<sub>4</sub>. (b) Crystal structure of K<sub>3</sub>Cu<sub>2</sub>O<sub>4</sub>, in different views. Light blue colour denotes copper(III), grey copper(II), dark blue potassium, red oxygen ions. (c) Coordination of K1 and K2 ions in K<sub>3</sub>Cu<sub>2</sub>O<sub>4</sub>.

long-range magnetic ordering at low temperatures with a  $\lambda$ -type anomaly. There are deviations from a  $T^3$ -Debye law at low temperatures, most likely due to magnon contributions to the heat capacity.

Following the analysis of the magnetic susceptibility (see below) we can assume that for a Heisenberg chain at temperatures  $T$  small compared to the intrachain spin exchange,  $J_{\text{intra}}$ ,

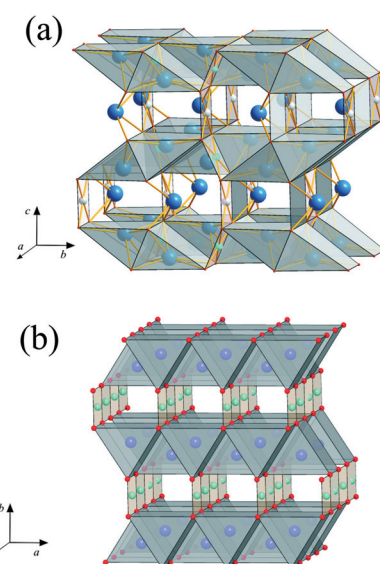


**Figure 3.** Comparison of the crystal structures of (a) K<sub>3</sub>Cu<sub>2</sub>O<sub>4</sub> and (b) KCuO<sub>2</sub>.

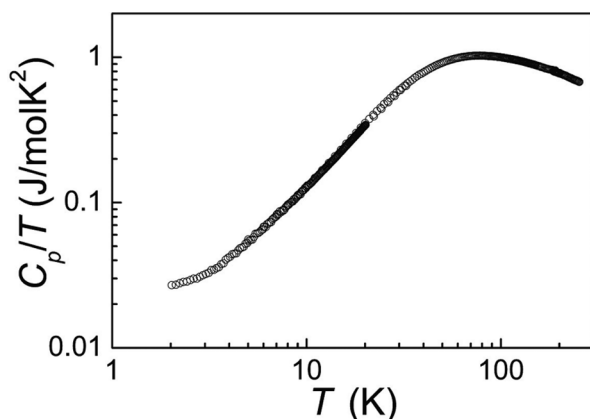


**Figure 4.** Specific heat of K<sub>3</sub>Cu<sub>2</sub>O<sub>4</sub>.

the magnon contributions are linear in  $T$  and can be represented by

$$C_{\text{mag}} = \frac{2}{3}R \frac{T}{J_{\text{intra}}}, \quad (3)$$

where  $R$  is the molecular gas constant. With  $J_{\text{intra}}$  as found from the analysis of the magnetic susceptibility one expects  $C_{\text{mag}}/T \approx 0.055 \text{ J}\cdot\text{mol}^{-1}\cdot\text{K}^{-2}$ ,

which is in fair agreement with the observed value of  $\approx 0.03 \text{ J}\cdot\text{mol}^{-1}\cdot\text{K}^{-2}$ .

A room temperature EPR spectrum obtained on a polycrystalline sample is displayed in Figure 5. We observe a spectrum with *g*-factors deviating from the free electron *g*-factor as is typically obtained for a Cu<sup>2+</sup> cation with copper in an elongated octahedron of oxygen atoms.

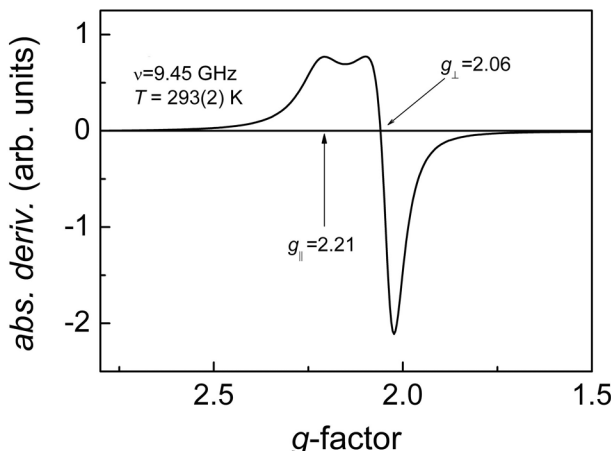


**Figure 5.** Room temperature X-band EPR powder spectrum of  $K_3Cu_2O_4$  with principal  $g$ -factors indicated.

The principal  $g$ -factors are found to be  $g_{\perp} = 2.06$  and  $g_{\parallel} = 2.21$  giving an averaged powder  $g$ -factor of  $g_{\text{pwd}} = (2g_{\perp} + g_{\parallel})/3 = 2.12$ .

The magnetic susceptibilities of  $K_3Cu_2O_4$  were measured for magnetic fields in the range 1 to 7 T. They are independent on the field strength in the temperature range 15–400 K, which indicates paramagnetic behaviour and negligible saturation of ferro- or ferrimagnetic impurities.

The susceptibility is characterised by a broad maximum centred at  $\sim 65$  K and Curie–Weiss law behaviour at high temperatures above  $\sim 200$  K with a negative Curie–Weiss temperature, which denotes predominant AFM spin-exchange interactions. The susceptibilities for  $T \geq 200$  K were fitted to a modified Curie–Weiss law (Figure 6) according to

$$\chi(T) = \chi_{\text{spin}}(T) + \chi_0, \quad (4)$$

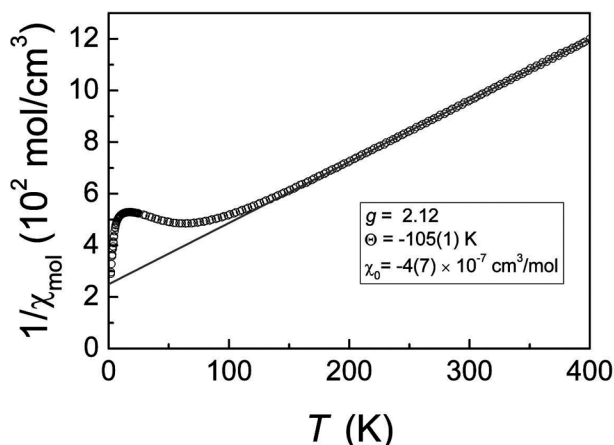


**Figure 6.** Inverse magnetic susceptibility and Curie–Weiss fit (solid line) for  $K_3Cu_2O_4$ . The fitted parameters,  $\Theta$  and  $\chi_0$ , are given in the inset. The  $g$ -factor was fixed to the value of 2.12.

In Equation (4) we consider the spin susceptibility according to

$$\chi_{\text{spin}}(T) = \frac{C}{T-\Theta}, \quad (5)$$

with the Curie constant,  $C = N_A g^2 \mu_B^2 S(S+1)/3k_B$ , and the Curie–Weiss temperature  $\Theta$ . The temperature independent part  $\chi_0$  comprises the diamagnetic susceptibilities of the closed shells, which have been summed up to  $-110 \times 10^{-6} \text{ cm}^3 \cdot \text{mol}^{-1}$  employing the increments given by Selwood<sup>[29]</sup> and the van Vleck contributions which are positive and of the same order of magnitude as the diamagnetic contributions. The van Vleck contributions are not known *a priori* to high precision, yet they can be estimated from the energy differences of the orbitals and the spin-orbit coupling constant and found typically of the order of the diamagnetic contribution ( $\sim 40\text{--}60 \times 10^{-6} \text{ cm}^3 \cdot \text{mol}^{-1}$ ). We used  $\chi_0$  as a fitting parameter and checked for its consistency. In the fits we have fixed the  $g$ -factor to the powder average of 2.12 as determined in the EPR measurements.

The fits converge very well to the parameters:

$$\Theta = -105(1) \text{ K}$$

$$\chi_0 = -4(7) \times 10^{-7} \text{ cm}^3 \cdot \text{mol}^{-1}$$

$$g = 2.12$$

$$\mu_{\text{eff}} = 1.84 \mu_B$$

The negative Curie–Weiss temperature indicates sizeable predominant AFM spin-exchange interaction. The fitted value of  $\chi_0$  is well in the range what may be expected with a compensation of the diamagnetic and the van Vleck temperature independent magnetic susceptibility.

The low-temperature susceptibility is characterised by a broad maximum centred at  $\sim 65$  K due to AFM short-range ordering consistent with the low dimensional behaviour, as expected from the crystal structure.

We now analyse the magnetic susceptibility in terms of a linear chain Heisenberg model. The fit of the experimental data to the susceptibility of a Heisenberg  $S = 1/2$  chain with uniform nearest-neighbour  $\text{Cu}^{2+}\cdots\text{Cu}^{2+}$  intrachain interaction ( $J_{\text{nn}}$ ) is shown in Figure 7. To account for a diverging contribution of a Curie-type susceptibility of impurities (“Curie-tail”) we subtracted from the experimental susceptibility a Curie contribution of  $\sim 1\%$  spin  $S = 1/2$  entities and obtained

$$\chi^*(T) = \chi_{\text{exp}}(T) - \chi_{\text{imp}} \quad (6)$$

$\chi^*(T)$  was fitted to an expression

$$\chi(T) = f\chi_{\text{spin}}(T) + \chi_0 \quad (7)$$

where the spin susceptibility,  $\chi_{\text{spin}}(T)$ , is given by the susceptibility of a  $S = 1/2$  Heisenberg chain as given by Johnston et al. as a Padé approximant to Quantum Monte Carlo and transfer-matrix density-matrix renormalisation group calculations.<sup>[30]</sup> Additionally, we have introduced a linear scaling factor  $f$ , which was found necessary to obtain acceptable fits. The  $g$ -factor has been fixed to the powder average determined in the EPR experiment.

The experimental data can be well described by a uniform Heisenberg chain with an AFM nearest-neighbour  $\text{Cu}^{2+}\cdots\text{Cu}^{2+}$  intrachain interaction  $J_{\text{nn}}$  of  $\sim 101$  K. The broad short-range ordering maximum peak at  $\sim 65$  K is in very good agreement with the ratio  $T_{\text{max}}/J = 0.6408$  as given by Johnston et al.<sup>[30]</sup>

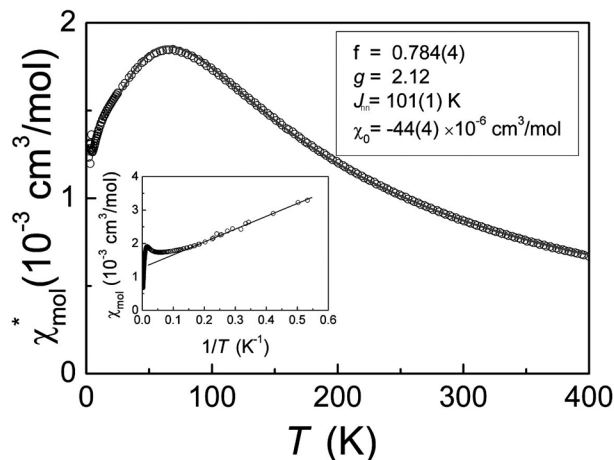


**Figure 7.** (Main frame) Magnetic susceptibility of  $K_3Cu_2O_4$  (o) fitted to the susceptibility of a  $S = 1/2$  Heisenberg chain with uniform nearest-neighbour  $Cu^{2+}\cdots Cu^{2+}$  intrachain spin exchange interaction (solid line). Fitted parameters are given in the upper inset. In order to obtain agreement between experiment and theory the susceptibility of the Heisenberg chain had to be multiplied by the factor  $f = 0.784(4)$ . Additionally, diamagnetic contributions from the closed shells and paramagnetic van Vleck contributions have been added up to the temperature independent term  $\chi_0$ . The lower inset displays the (uncorrected) susceptibility of  $K_3Cu_2O_4$  (o) vs. the inverse temperature. The linear increase towards low temperatures has been attributed to the susceptibility of impurities. From the slope we estimate the amount of  $S = 1/2$  impurities to about 1 % of the sample.

There is, however, disagreement between the magnitudes of the experimental susceptibility at  $T_{\max}$ . Theoretically, one expects a value which is about 20 % higher. Efforts to attribute this discrepancy to an additional next-nearest neighbour intrachain spin exchange interaction ( $J_{nnn}$ ), by introducing a mean-field type renormalisation of the susceptibility were not conclusive. A comparison of the experimental data with the exact diagonalisation results by Heidrich-Meissner et al.<sup>[31]</sup> indicated a ratio of  $-0.25 < \alpha = J_{nnn}/J < 0.25$ , with a clear preference to  $\alpha \approx 0$ , i.e. negligible next-nearest neighbour interaction. This finding supports the fit of the spin susceptibility with a nearest-neighbour Heisenberg chain model and proves the non-magnetic state of the  $Cu^{3+}$  cations.

## Conclusions

In comparison to the analogue sodium cuprates synthesised with the azide/nitrate route ( $Na_3Cu_2O_4$ ,  $Na_8Cu_5O_{10}$ ), substitution of the potassium ion in the structure had an influence on dihedral angles between adjacent  $CuO_4$  square units, which led to formation of undulating  $^1_{\infty}CuO_2$  chains in  $K_3Cu_2O_4$ .  $K_3Cu_2O_4$  is isostructural to  $K_3Ni_2O_4$  and  $K_3Pt_2O_4$ <sup>[26]</sup> and the shortest Cu–Cu distance between two  $^1_{\infty}CuO_2$  chains is  $\sim 5.4$  Å, which is in agreement with the respective value in  $K_3Ni_2O_4$ . In  $K_3Pt_2O_4$ , these distances are just slightly higher (5.5 Å). Although, all three compounds have the same chain arrangement, and contain transition metal ions with unpaired spins, only  $K_3Cu_2O_4$  shows low dimensional magnetic behaviour. The analysis of the magnetic susceptibility proves that

$K_3Cu_2O_4$  realises a  $S = 1/2$  chain system. Inclusion of nearest-neighbour spin-exchange interactions suffices to describe the temperature dependence of the susceptibility adequately. There is no indication for sizeable next-nearest neighbour interaction. In view of the crystal structure, which indicates an ordered  $\cdots Cu^{3+}\cdots Cu^{2+}\cdots Cu^{3+}\cdots Cu^{2+}\cdots$  arrangement along the chain, the nearest-neighbour spin exchange couples  $Cu^{2+}$  entities. The magnitude of the spin exchange interaction is somewhat lower than that found for the analogue compound  $Na_3Cu_2O_4$  (about 40 %). Like for  $Na_3Cu_2O_4$ , next-nearest neighbour spin exchange ( $J_4$  in the notation of<sup>[14]</sup>) appears to be negligible. It amounted to about 10 % for  $Na_3Cu_2O_4$ . In contrast to  $Na_3Cu_2O_4$ , which exhibits long-range ordering at  $\sim 23$  K,<sup>[32]</sup> according to our heat capacity data  $K_3Cu_2O_4$  shows no indication of long-range three-dimensional magnetic ordering down to 2 K. This can be understood as due to the increased inter-chain interaction through the shortest Cu–Cu distances in  $K_3Cu_2O_4$ ,  $\sim 5.4$  Å as compared to  $\sim 4.2$  Å in  $Na_3Cu_2O_4$ . Additionally, as already pointed out by Horsch et al.,<sup>[14]</sup> the inter-chain coupling is strongly affected by geometrical frustration, which can suppress long-range ordering, since the  $^1_{\infty}CuO_2$  chains are arranged in a honeycomb lattice in the  $a, b$  plane (Figure 2b). There is an apparent discrepancy between the high-temperature behaviour of the magnetic susceptibility, characterised by a Curie–Weiss temperature of  $\sim -105$  K and a  $g$ -factor of 2.12, and the low-temperature behaviour, which is in well agreement with the susceptibility, of a  $S = 1/2$  Heisenberg chain with nearest-neighbour AFM spin interaction. The spin-exchange found by fitting the susceptibility to the Heisenberg chain theory indicates an AFM spin-exchange of  $\sim 101$  K. This leads, in case of a uniform chain with two neighbours for each spin, to a Curie–Weiss temperature of  $\Theta = -J_{nn}/2 \sim -50$  K. The respective required interchain interactions appear to be too small to move this value significantly towards the Curie–Weiss temperature found by fitting the high-temperature susceptibility. Such large interchain interactions would lead to long-range ordering at elevated temperatures, which has not been observed experimentally.

## Acknowledgement

We thank J. Nuss for collecting X-ray single-crystal data and helping with the single crystal structure solution, P. Reuvekamp for the measurement of magnetic properties as well as G. Siegle for providing the specific heat measurement.

## References

- [1] K. M. Shen, J. C. S. Davis, *Mater. Today* **2008**, *11*, 14–21.
- [2] L. P. Gorkov, V. Z. Kresin, *Phys. Rep.* **2004**, *400*, 149–208.
- [3] Hk. Müller-Buschbaum, *Angew. Chem.* **1989**, *101*, 1503–1524; *Angew. Chem. Int. Ed. Engl.* **1989**, *28*, 1472–1493.
- [4] Hk. Müller-Buschbaum, *Angew. Chem.* **1991**, *103*, 741–761; *Angew. Chem. Int. Ed. Engl.* **1991**, *30*, 723–744.
- [5] C. Kim, Z. X. Shen, N. Motoyama, H. Eisaki, S. Uchida, T. Tohyama, S. Maekawa, *Phys. Rev. B* **1997**, *56*, 15589–15595.
- [6] S. Park, Y. J. Choi, C. L. Zhang, S. W. Cheong, *Phys. Rev. Lett.* **2007**, *98*, 057601–057604.
- [7] M. Hase, I. Terasaki, K. Uchinokura, *Phys. Rev. Lett.* **1993**, *70*, 3651–3654.

- [8] D. Trinschek, M. Jansen, *Angew. Chem.* **1999**, *111*, 234–235; *Angew. Chem. Int. Ed.* **1999**, *38*, 133–135.
- [9] S. Pfeiffer, J. Nuss, M. Jansen, *Z. Anorg. Allg. Chem.* **2010**, *636*, 23–29.
- [10] J. Nuss, S. Pfeiffer, S. V. Smalalen, M. Jansen, *Acta Crystallogr. Sect. B* **2010**, *66*, 27–33.
- [11] S. Pfeiffer, J. Nuss, M. Jansen, *Z. Kristallogr. New Cryst. Struct.* **2009**, *224*, 163–164.
- [12] M. Sofin, E. M. Peters, M. Jansen, *J. Solid State Chem.* **2005**, *178*, 3708–3714.
- [13] N. Z. Ali, J. Sirker, J. Nuss, P. Horsch, M. Jansen, to be published.
- [14] P. Horsch, M. Sofin, M. Mayr, M. Jansen, *Phys. Rev. Lett.* **2005**, *94*, 0764031–0764034.
- [15] L. Capogna, M. Reehuis, A. Maljuk, R. K. Kremer, B. Ouladdiaf, M. Jansen, B. Keimer, *Phys. Rev. B* **2010**, *82*, 0144071–0144076.
- [16] D. Fischer, W. Carl, H. Glaum, R. Hoppe, *Z. Anorg. Allg. Chem.* **1990**, *585*, 75–81.
- [17] R. Hoppe, W. Losert, *Z. Anorg. Allg. Chem.* **1985**, *521*, 69–78.
- [18] A. Möller, *Z. Anorg. Allg. Chem.* **2001**, *627*, 1192–1198.
- [19] K. Hestermann, R. Hoppe, *Z. Anorg. Allg. Chem.* **1969**, *367*, 249–260.
- [20] G. Brauer, *Handbuch der Präparativen Anorganischen Chemie*, Ferdinand Enke Verlag, **1978**, p. 950–954.
- [21] TOPAS 3.0, Bruker AXS GmbH, Karlsruhe, Germany.
- [22] SMART, Bruker Molecular Analysis Research Tool, version 5.632, Bruker AXS Inc., Madison, WI, USA, **1997**.
- [23] G. M Sheldrick: *SADABS*, Bruker AXS area detector scaling and absorption, version 2008/1, University of Göttingen, Germany, **2008**.
- [24] G. M. Sheldrick, *Acta Crystallogr. Sect. A* **2008**, *64*, 112–122.
- [25] H. Lueken, *Magnetochemistry*, Teubner, Stuttgart **1999**, p. 426–427.
- [26] H. Zentgraf, K. Claes, R. Hoppe, *Z. Anorg. Allg. Chem.* **1980**, *462*, 92–105.
- [27] Further details may be obtained from Fachinformationszentrum Karlsruhe, 76344 Eggenstein-Leopoldshafen, Germany (Fax: +49-7247-808-666; E-Mail: [crysdata@fiz-karlsruhe.de](mailto:crysdata@fiz-karlsruhe.de), [http://www.fiz-karlsruhe.de/request\\_for\\_deposited\\_data.html](http://www.fiz-karlsruhe.de/request_for_deposited_data.html)) on quoting the deposition number CSD-380487.
- [28] R. Hoppe, *Z. Kristallogr.* **1979**, *150*, 23–52.
- [29] P. W. Selwood, *Magnetochemistry*, Interscience, New York, **1956**, p. 78.
- [30] D. C. Johnston, R. K. Kremer, M. Troyer, X. Wang, A. Klümper, S. L. Bud'ko, A. F. Panchula, P. Canfield, *Phys. Rev. B* **2000**, *61*, 9558–9606.
- [31] F. Heidrich-Meisner, A. Honecker, T. Vekua, *Phys. Rev. B* **2006**, *74*, 0204031–020404.
- [32] M. Sofin, Dissertation, University Stuttgart, Germany, **2003**.

Received: January 13, 2011

Published Online: February 17, 2011